Inorganic Chemistry

pubs.acs.org/IC

Article

Interlinker Hydrogen Bonds Govern CO_2 Adsorption in a Series of Flexible 2D Diacylhydrazone/Isophthalate-Based MOFs: Influence of Metal Center, Linker Substituent, and Activation Temperature

Kornel Roztocki, Monika Szufla, Volodymyr Bon, Irena Senkovska, Stefan Kaskel, and Dariusz Matoga*

Cite This: *Inorg. Chem.* 2020, 59, 10717−10726

Read Online

ACCESS | Metrics & More | Article Recommendations | Supporting Information

ABSTRACT: Four new layered flexible metal−organic frameworks (MOFs) containing a diacylhydrazone moiety, namely, guest-filled $[Zn_2(iso)_2(tdih)_2]_n$ (**1**), $[Zn_2(NH_2iso)_2(tdih)_2]_n$ (**2**), $[Cd_2(iso)_2(tdih)_2]_n$ (**3**) and $[Cd_2(NH_2iso)_2(tdih)_2]_n$ (**4**) were synthesized using terephthalaldehyde di-isonicotinoylhydrazone (*tdih*) as a linear ditopic linker as well as isophthalate (iso) or 5-aminoisophthalate (NH_2iso) as angular colinkers. The MOFs with hexacoordinated cadmium centers feature two-dimensional pore systems as compared to the MOFs with pentacoordinated zinc centers showing either zero-dimensional or mixed zero-/one-dimensional voids, as evidenced by single-crystal X-ray diffraction. In contrast to the frameworks based on isophtalates which do not show any significant gas uptakes, introduction of amino-substituted linker enables CO_2 adsorption. Gently activated aminoisophthalate-based frameworks, that is, guest-exchanged in methanol and heated to 100 °C, show reversible gated CO_2 adsorptions at 195 K, whereas the increase of activation temperature to 150 °C or more leads to one-step isotherms and lower adsorption capacities. X-ray diffraction and IR spectroscopy reveal significant structural differences in interlayer hydrogen bonding upon activation of materials at higher temperatures. The work emphasizes the role of hydrogen bonds in crystal engineering of layered materials and the importance of activation conditions in such systems.

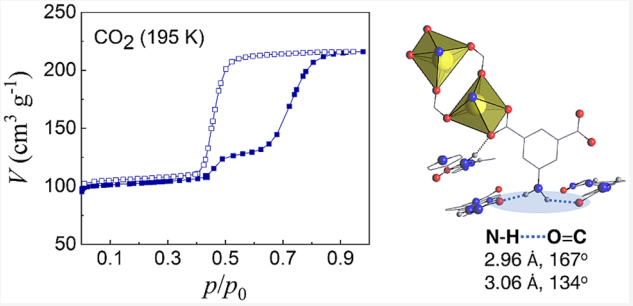

INTRODUCTION

Crystalline materials that respond through structural changes to external chemical or physical stimuli, such as specific compounds,[1,2] pressure,[3] mechanical force,[4,5] electrical field,[6] or electromagnetic radiation[7] are highly desirable for smart devices and are useful for studying stimulus-structure−property relationships. Among such materials, stimuli-responsive crystalline porous coordination polymers[8] called flexible metal−organic frameworks are a significant group that is intensively explored.[9−11] The intrinsic response of flexible MOFs to external conditions, after local initiation, propagates through the crystalline lattice with retention of long-range order. Different nanoflexibility modes such as swelling,[12] breathing,[13] linker rotation[14]/bending,[15] change of interpenetration level,[16] and subnetwork displacement for 3D catenated networks[17] or stacked[18]/interdigitated[19,20] layers drive macroscopic changes of flexible MOFs as well as govern several distinct phenomena such as gate opening,[21] negative gas adsorption,[15] pronounced usable capacity,[22] chemical control of structures,[23] continuous-breathing behavior,[24] collective breathing,[25] self-accelerating sorption,[26] shape memory effect,[27] proton conductivity,[28] and solvent-induced magnetic ordering.[29]

The stimuli-responsive nature of flexible MOFs makes their study challenging. For instance, the most commonly used techniques for structural investigations, that is, X-ray diffraction (XRD), require maintaining the crystallinity and crystal integrity (single-crystal XRD) which cannot be fulfilled by numerous samples of flexible MOFs suffering from stress during activation and adsorption processes. As alternative or complementary techniques, infrared and Raman spectroscopy have proved to be useful for structural investigations of rigid and flexible MOFs. Valuable insights into MOF structures provided by vibrational spectroscopy have been made while studying, for instance, defects in UiO-66,[30] activation and reactivity of Pt-UiO-67,[31] post-synthetic modification,[32] gas interactions with open metal sites,[33,34] cooperative adsorption properties,[35] reaction progress in solid state,[36,37] structural dynamics,[38] TCNQ (7,7,8,8-tetracyanoquinodimethane) ordering[39] or NH_3 adsorption[40] in HKUST-1, vibrational

Received: April 21, 2020
Published: July 14, 2020

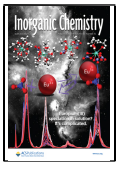

Scheme 1. Synthetic Route to Metal−Organic Frameworks 1-4[a]

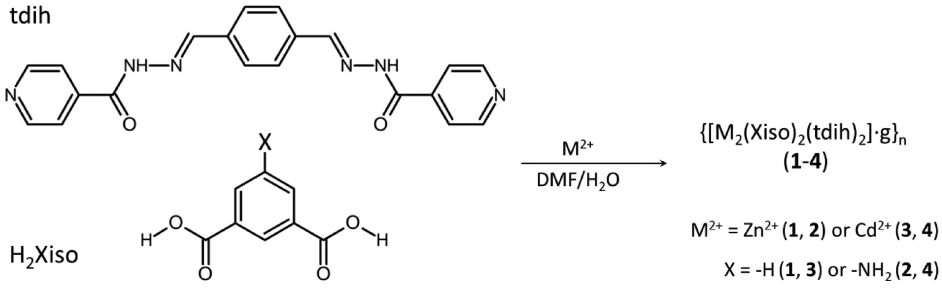

[a]Abbreviations used: tdih, terephthalaldehyde di-isonicotinoylhydrazone; g, guest molecules; H_2Xiso, isophthalic acid (X = H) or 5-aminoisophthalic acid (X = NH_2).

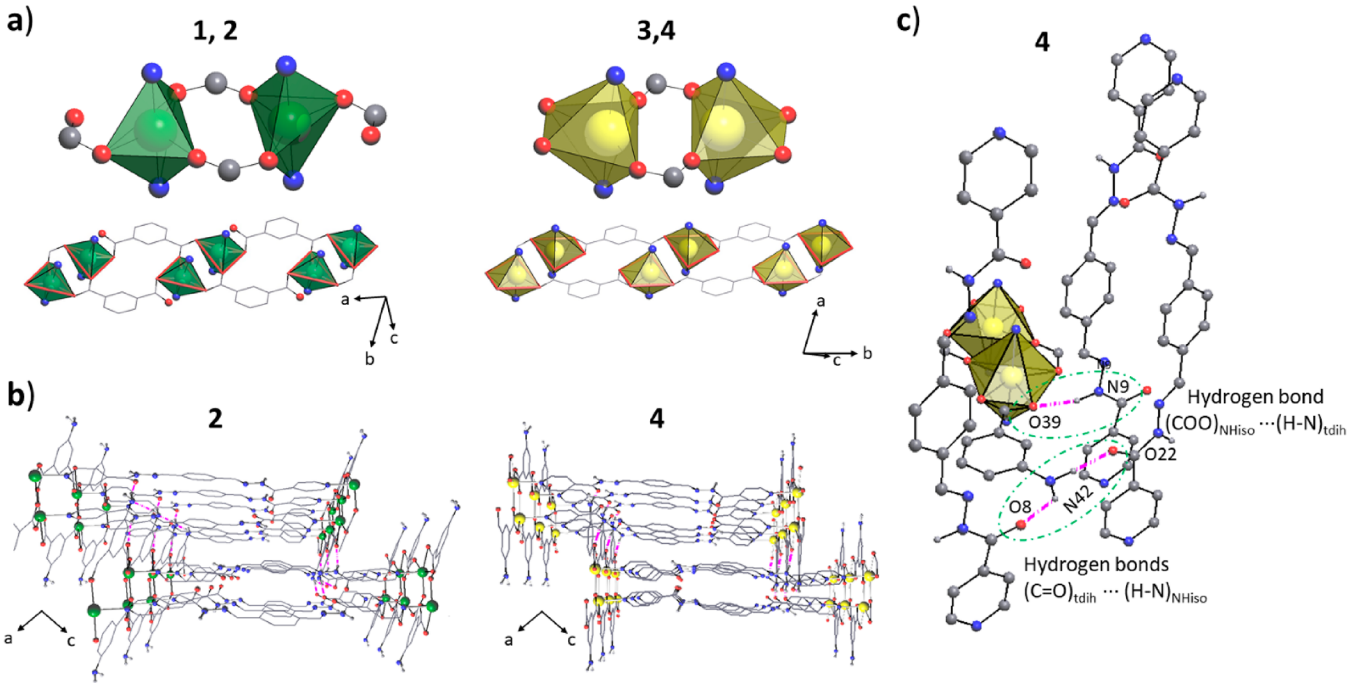

Figure 1. X-ray crystal structures of MOFs **1**−**4**. (a) Coordination environments of dizinc (**1**, **2**) and dicadmium SBU (**3**, **4**) and representation of 1D chains $[M_2(Xiso)_2]_n$ cross-linked by *tdih* to form 2D layers. (b) Interdigitated layers of **2** and **4** in a perspective view along the *b*-axis. (c) Hydrogen bonds in **4** involving acylhydrazone moiety (*tdih*) and COO or NH_2 groups of NH_2iso colinker. All hydrogen atoms except those attached to nitrogen are omitted for clarity. C, gray; H, light gray; N, blue; O, red; Zn, green; and Cd, yellow.

fingerprint of MIL-53(Al),[41] and CO_2 adsorption[42,43] and paddle-wheel deformability in DUT-8(Ni, Co).[44] Moreover, as can be seen from the above examples, major scientific efforts concerning flexible MOFs are directed toward understanding of 3D materials,[9−11,45,46] and the reports on 2D materials are still relatively rare and sought after.[20,42,47−51]

In this work we report the synthesis, single-crystal XRD elucidated structures and adsorption properties of a series of four new two-dimensional MOFs whose layers are stabilized by N−H···O hydrogen bonds. All zinc- or cadmium-based frameworks, $[M_2(Xiso)_2(tdih)_2]$, contain a diacylhydrazone linear ditopic linker, terephthalaldehyde di-isonicotinoylhydrazone (*tdih*), and isophtalate (X = H) or 5-aminoisophthalate (X = NH_2) angular colinkers. We demonstrate that interlayer hydrogen bonds involving the diacylhydrazone linker have a considerable impact on porous structures as well as gas adsorption properties. Introduction of amino substituents into isophthalate colinkers induces gating type flexibility in the resulted MOFs. This dynamic behavior is controlled by desolvation conditions that either preserve or change initial interlayer hydrogen bond networks as collectively evidenced by powder X-ray diffraction (PXRD), thermogravimetric analysis (TGA), and infrared (IR) spectroscopy. A diversity of key interlayer hydrogen bond networks governing activation and adsorption properties of the frameworks result from dual character (−CO═N—NH−) of the diacylhydrazone moiety that either acts as a hydrogen bond donor or an acceptor dependently on the colinker used. It is also noteworthy that the approach presented here, to functionalize a layered MOF with terminal NH_2 groups by replacing linkers with their amino analogues, is not always successful. For example, such replacement of isophthalate in a 2D MOF, $[Zn_2(iso)_2(bpy)_2]_n$ (bpy = 4,4′- bipyridine) led to a nonporous 3D coordination polymer, $[Zn(NH_2iso)(bpy)]_n$, with coordinated NH_2 groups.[52] In contrast, however, this approach yielded a layered zinc-based MOF with pendant NH_2 groups when bpy was replaced with 4-pyridinecarboxaldehyde isonicotinoyl hydrazone (*pcih*).[42] This observation underscores the role of hydrogen-bond acceptors, present in acylhydrazones, capable of involving NH_2 groups in hydrogen bonding.

https://dx.doi.org/10.1021/acs.inorgchem.0c01182
Inorg. Chem. 2020, 59, 10717−10726

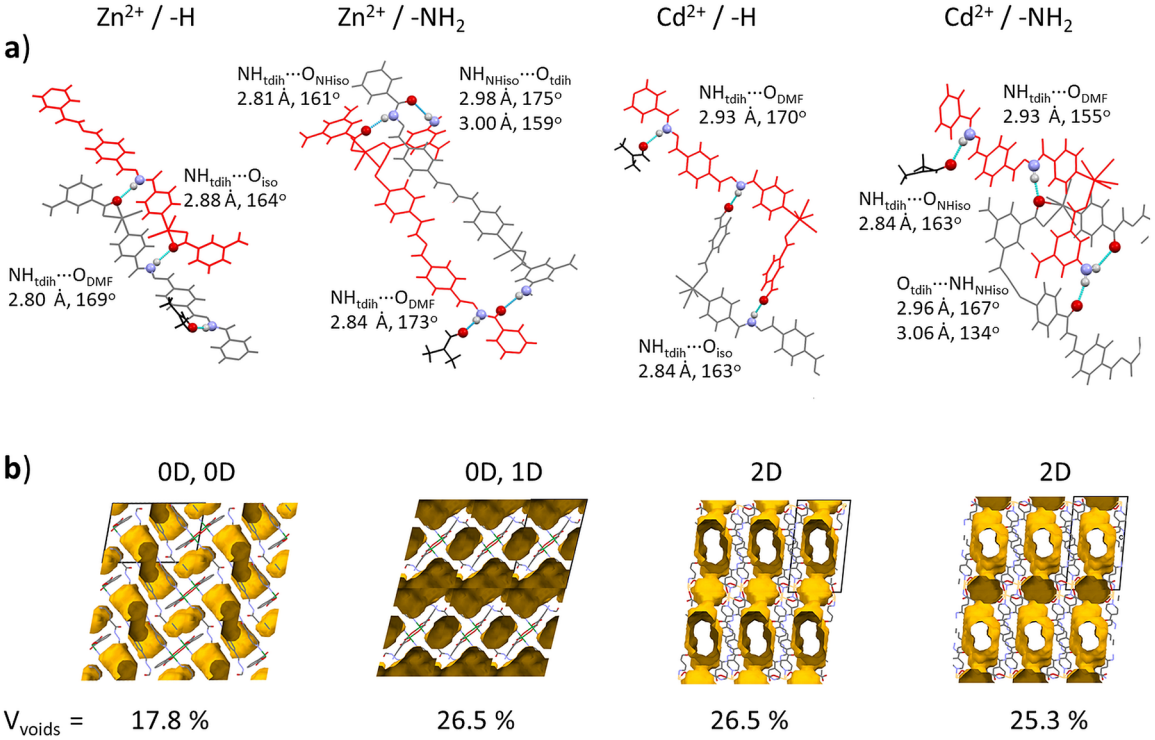

Figure 2. Supramolecular interactions involving adjacent layers in the $\{[M_2(X\text{-iso})_2(tdih)_2]\cdot guest\}_n$ family (**1**, **2**, **3b**, and **4**, respectively). (a) Schematic representation of intermolecular interactions involving two adjacent layers and solvent molecules. (b) Contact surface and fraction of voids (V_{voids}) were calculated with Mercury software by using a probe molecule with a radius of 1.2 Å (views along the *a*-axis).

RESULTS AND DISCUSSION

Synthesis and Structure. A series of four two-dimensional (2D) diacylhydrazone-carboxylate metal−organic frameworks $\{[M_2(Xiso)_2(tdih)_2]\cdot g\}_n$ (g = guest molecules, M = Zn or Cd), namely, guest-filled $[Zn_2(iso)_2(tdih)_2]_n$ (**1**), $[Zn_2(NH_2\text{iso})_2(tdih)_2]_n$ (**2**), $[Cd_2(iso)_2(tdih)_2]_n$ (**3**, **3b**), and $[Cd_2(NH_2\text{iso})_2(tdih)_2]_n$ (**4**), have been synthesized with good yields (64−75%) from a metal nitrate, terephthalaldehyde di-isonicotinoylhydrazone (*tdih*) as a linear ditopic linker as well as isophtalic ($isoH_2$) or 5-aminoisophthalic acids (NH_2isoH_2) as an angular colinker precursors (Scheme 1 and Experimental Section). The structures of all compounds were determined by single-crystal X-ray diffraction carried out on crystals selected from bulk samples. The identity and purity of **1**−**4** and **3b** was corroborated by elemental analyses, powder X-ray diffraction, and thermogravimetric analysis (Figures S1−S2). In the case of $[Cd_2(iso)_2(tdih)_2]_n$, two crystal structures (**3** and **3b**) were elucidated (Figure S3), and the latter was used for comparison with other structures. The only differences between the structures lie in the geometry of $[Cd_2\ iso_2]_n$ chains and the mutual position of adjacent layers which is affected by different numbers of interlayer solvent molecules.

As revealed by X-ray diffraction, all MOFs crystallize in the triclinic system (space group $P\bar{1}$) with the asymmetric unit containing one metal cation, one isophthalate anion ($Xiso^{2-}$), and guest molecules 1DMF (**1**, **2**, **4**) or 2DMF (**3b**), and one *tdih* linker. All frameworks show the uniform *sql* topology,[53] and the coordination geometry of metals can be described as either a disordered pentagonal bipyramidal (**1**, **2**) or a disordered octahedral (**3b**, **4**; Table S1). Carboxylates of $Xiso^{2-}$ linkers and metal ions form dinuclear secondary building units $M_2(COO)_2$ (SBUs) with intermetallic M···M distances of 4.11, 4.05, 4.06, and 4.07 Å for **1**−**4**, respectively (Figure 1).

The $Xiso^{2-}$ ions act as μ_3-$\kappa^1\kappa^1\kappa^1$ (**1**, **2**) or μ_3-$\kappa^2\kappa^1\kappa^1$ (**3b**, **4**) linkers and connect $M_2(COO)_2$ SBUs into 1D ladder chains $[M_2(Xiso)_2]$ running along the *a*- (**1**, **2**) or *b*-axis (**3b**, **4**). These chains are further bridged by *tdih* linkers, adopting either *trans* (**1**) or *cis* (**2**-**4**) configurations, to form 2D layers (Figures S4−S6). These interdigitated layers are stacked and held together via direct interlayer and layer-guest hydrogen bonds as well as by $\pi-\pi$ interactions (Figure 2 and Figures S4−S6 and Tables S2 and S3). In the frameworks based on unsubstituted isophthalates (**1**, **3b**) only one type of hydrogen bond between adjacent layers is observed: $(N-H)_{tdih}\cdots O_{isophthalate}$ with distances *d*(N9−H9···O39) = 2.88 or 2.84 Å and angles equal to 164 or 163°, for **1** and **3b**, respectively. Additionally, DMF molecules are involved in hydrogen bonding with the acylhydrazone NH group of *tdih* ligands with *d*(N20−H20···O47) = 2.80 or 2.93 Å and corresponding angles of 169 or 170° for **1** and **3b**, respectively. On the other hand, the presence of amino functional group in **2** and **4** has a considerable impact on a number of hydrogen bonds. Apart from $(N-H)_{tdih}\cdots O_{isophthalate}$ hydrogen bonds (*d*(N9−H9···O39) = 2.81 or 2.84 Å with angles equal to 161 or 163° for **2** and **4**, respectively) and $(N-H)_{tdih}\cdots O_{DMF}$ hydrogen bonds, these frameworks are stabilized by additional hydrogen bonds between acylhydrazone oxygen atoms and amino group hydrogen atoms from the NH_2iso^{2-} ion which have a significant influence on gas adsorption properties, discussed in detail below. Independent of the hydrogen bonds occurrence, there are two extra types of moderate $\pi-\pi$ interactions between aromatic rings of a layer and two adjacent layers present in all structures (Table S2 and Figure S5). It is

https://dx.doi.org/10.1021/acs.inorgchem.0c01182
Inorg. Chem. 2020, 59, 10717−10726

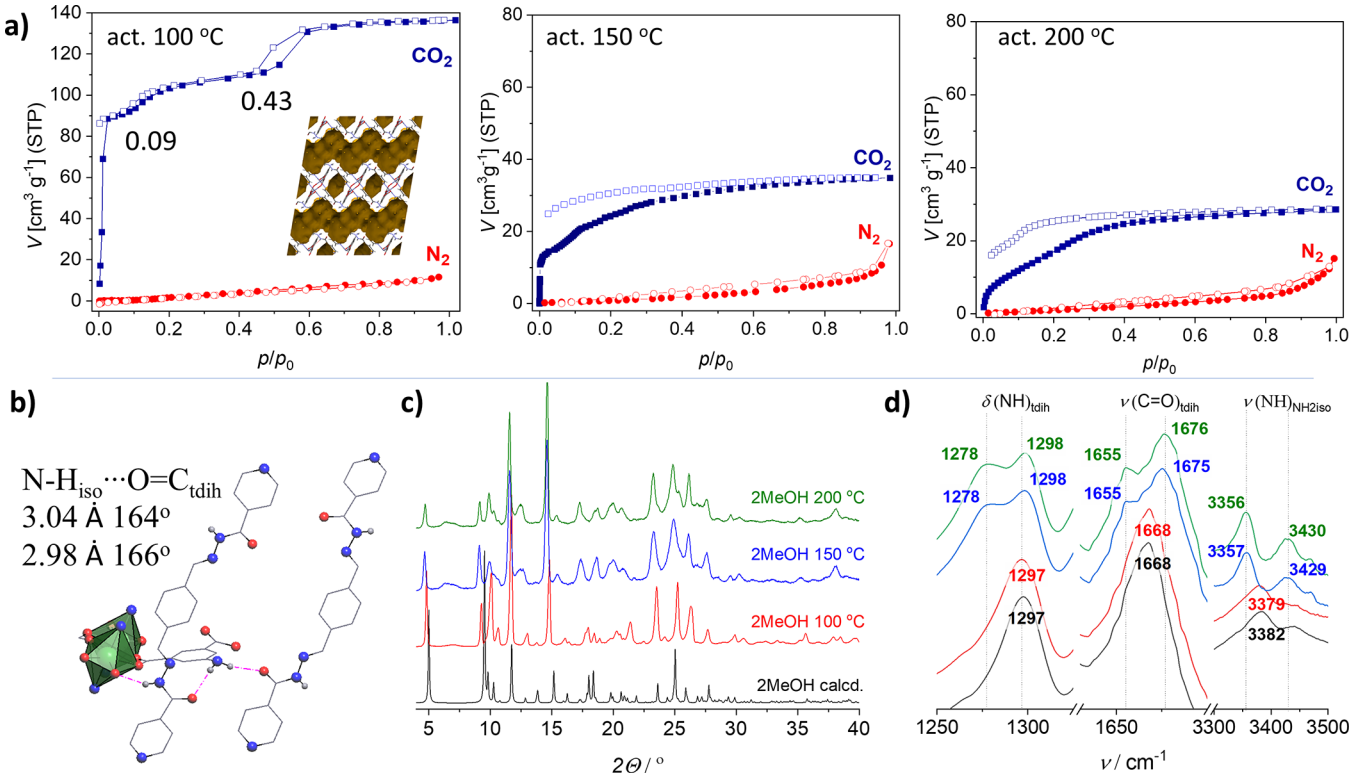

Figure 3. (a) N_2 (77 K) and CO_2 (195 K) physisorption isotherms for **2MeOH** activated at different temperatures (100, 150, and 200 °C) (adsorption, full symbols; desorption, empty symbols.) (b) Hydrogen bonds between NH_2 of aminoisophthalate and C═O of the *tdih* colinker in **2MeOH**: red−oxygen, gray−carbon, blue−nitrogen, pale gray−hydrogen, H atoms (except those bound to N) are omitted for clarity. (c) Comparison of PXRD patterns between **2MeOH** (calculated based on SC-XRD at 100 K) and **2MeOH** activated at different temperatures (the patterns for activated materials were collected in inert atmosphere at RT). (d) IR spectra corresponding to PXRD patterns (the same color codes).

facilitated by doubly pillared network nodes and close arrangement of layers (Figure S6).

The interplay between metal type and isophthalate colinkers in the assembly of diacylhydrazone-based frameworks is responsible for creation of pores of various dimensionalities which occupy 17.8 to 26.5% of unit cell volumes (Figure 2). Compound **1** based on iso^{2-} and Zn^{2+} ions has two types of 0D pores, whereas replacing of iso^{2-} by NH_2iso^{2-} leads to a mixed 0D and 1D pore system (**2**). On the other hand, independent of the isophthalate used, both cadmium-based MOFs **3** and **4** possess two-dimensional pore structures. Furthermore, the *tdih* linker in MOF **1** has *trans* configuration as compared to MOFs **2**−**4** in which it adopts *cis* configuration (Figure S4).

As revealed by thermogravimetric analysis, the as-synthesized materials **1**−**4** undergo gradual guest removal (water up to ca. 120 °C followed by DMF) already at the onset of heating and without reaching a distinct plateau (except for **1**), which is followed by decomposition observed for all frameworks above ca. 300 °C (Figure S2). Complementary variable temperature PXRD measurements (Figures S7−S10) confirm that the removal of guest molecules from the as-synthesized frameworks based on unsubstituted isophthalate (**1** and **3**) leads mostly to a gradual decrease of intensities of peaks and their slight broadening, which begins from ca. 240 or 200 °C, for **1** and **3**, respectively. In contrast, however, the PXRD patterns of MOFs with aminoisophthalate colinkers (**2** and **4**) demonstrate that these materials undergo phase transitions already above ca. 140 °C (Figures S7−S10) before they decompose. These transitions are associated with interlayer rearrangements since IR spectra show that indicative intraframework bands remain intact (e.g., asymmetric and symmetric stretching bands of carboxylates) upon thermal activation at 200 °C and 10 mbar (Figures S11 and S12).

Given the hydrophilic nature of acylhydrazones exhibiting high capability of hydrogen bond formation due to the presence of both donor (N−H) and acceptor groups (C═O) (Figure S13), we have also characterized the hydrolytic stability of materials **1**−**4** by analyzing these solids after immersion in water for at least 72 h at room temperature. Unlike in the archetypical hydrolyzable Zn-based MOF-5,[54] we have observed that all d^{10} metal-based MOFs **1**−**4** exchange DMF guest molecules by water (MOFs after the exchange are denoted as $\mathbf{1H_2O}$−$\mathbf{4H_2O}$) with retention of intralayer bonding and thermal stability up to 300 °C. This is collectively evidenced by elemental (Experimental Section) and thermogravimetric analyses (Figure S14), powder X-ray diffraction, and IR spectroscopy (Figures S11 and S12). The PXRD patterns of $\mathbf{1H_2O}$−$\mathbf{4H_2O}$ clearly demonstrate that new crystalline phases appear after soaking in water, and main differences observed for all MOFs in IR spectra are found in the characteristic regions of stretching N—H and C═O bands, which indicates changes in hydrogen bonding. Additionally, in the case of zinc-based water-exchanged MOFs, the differences between the bands corresponding to asymmetric (and symmetric for **2**) stretching of carboxylates are observed, which point to intralayer rearrangements upon soaking in water. Analogous control experiments carried out for a known representative of interdigitated layered MOFs, that is, CID-1 ($\{[Zn_2(iso)_2(bpy)_2]\cdot DMF\}_n$) not containing hydrogen bond

https://dx.doi.org/10.1021/acs.inorgchem.0c01182
Inorg. Chem. 2020, 59, 10717−10726

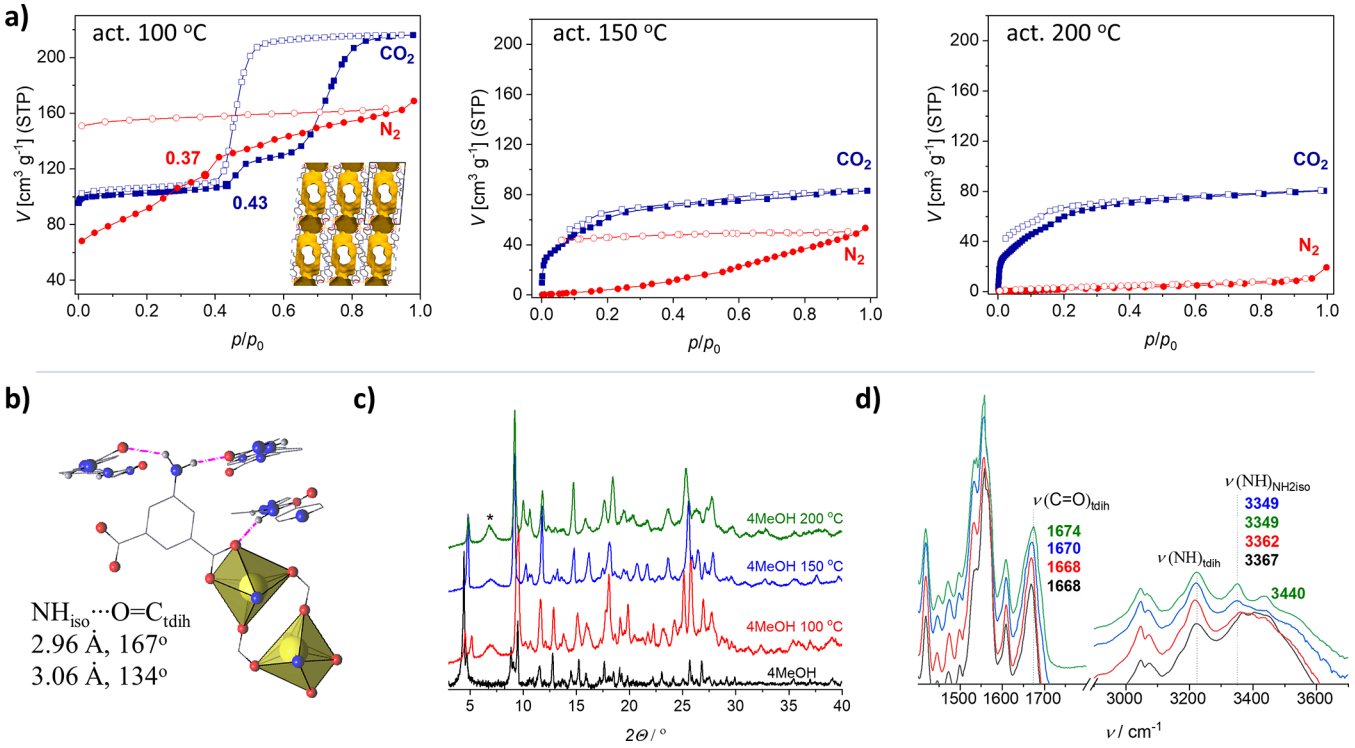

Figure 4. (a) N_2 (77 K) and CO_2 (195 K) physisorption isotherms for **4MeOH** activated at different temperatures (100, 150, and 200 °C) (adsorption, full symbols; desorption, empty symbols). (b) Hydrogen bonds between NH_2 of aminoisophthalate and C═O of *tdih* colinker in **4**: red—oxygen, gray—carbon, blue—nitrogen, pale gray—hydrogen, H atoms (except those bound to N) are omitted for clarity. (c) Comparison of PXRD patterns between **4MeOH** (calculated based on SC-XRD at 100 K) and **4MeOH** activated at different temperatures (the patterns for activated materials were collected in inert atmosphere at RT, *broad peak at ~6° is the artifact from a sample holder). (d) IR spectra corresponding to PXRD patterns (the same color code).

Table 1. Porosity Parameters for MOFs 1—4

structural parameters				sorption parameters					
MOF	p_{ws} [Å]	m_{pd} [Å]	V_{pt} [$cm^3\ g^{-1}$]	MOF	T_{act} [°C]	p/p_0 CO_2	V_{pe} (CO_2) [$cm^3\ g^{-1}$]	p/p_0 N_2	V_{pe} (N_2) [$cm^3\ g^{-1}$]
1	1.77	4.32	0.126	–	–	–	–	–	–
2	2.64	4.65	0.194	–	–	–	–	–	–
2MeOH	2.72	4.52	0.167	**2MeOH**	100	0.09	0.167		
						0.43	0.196	–	–
						0.98	0.244	–	–
3	3.40	5.58	0.177	**3MeOH**	50	0.99	0.120	–	–
4	3.54	5.64	0.184	**4MeOH**	100	0.43	0.189	0.37	0.179
						0.59	0.231	0.98	0.262
						0.98	0.386	–	–
					150	0.98	0.148	0.98	0.074
					200	0.98	0.144	–	–

[a] p_{ws}, pore windows size (Zeo++);[55] m_{pd}, maximum pore diameter (Zeo++); V_{pt}, theoretical pore volume (Mercury 3.10.2); $V_{pe}(CO_2)$ and $V_{pe}(N_2)$, experimental pore volume derived from CO_2 (195 K) and N_2 (77 K) adsorption isotherms, respectively; p/p_0, relative pressure.

donors and acceptors,[19] have shown that its hydrophobic pores prevent interlayer DMF exchange for water (Figure S15). This emphasizes the importance of polar groups present in acylhydrazones for hydrolytic stability of MOFs.

Adsorption Properties. Free voids in the as-synthesized MOFs **1**—**4** are mostly occupied by DMF molecules interacting strongly with polar walls through hydrogen bonds (Figure 2). As shown in VT-PXRD patterns (Figures S7—S10) and IR spectra (Figures S11 and S12), direct thermal activation is responsible for structural changes arising from destabilization of subtle hydrogen bonding networks, which are observed already above 140 °C for **2** and **4**. To enable gentle activation conditions, DMF molecules were exchanged by methanol (MeOH) as a solvent with a lower boiling point. Soaking the as-synthesized materials in MeOH for 1—2 days removed DMF molecules from all materials except **1** (Figures S16—S18), most likely due to hindered diffusion in 0D voids (MOFs after the exchange are denoted as **1MeOH**—**4MeOH**).

The frameworks based on unsubstituted isophthalates (**1** and **3**), independently of activation conditions, are practically not porous toward N_2 at 77 K and CO_2 at 195 K. They adsorb only small amounts (Figures S19—S21), whereby the highest amounts of adsorbed CO_2, reaching 70 $cm^3\ g^{-1}$ (STP), were observed for **3MeOH** activated at 50 °C. In contrast, however,

https://dx.doi.org/10.1021/acs.inorgchem.0c01182
Inorg. Chem. 2020, 59, 10717—10726

the aminoisophthalate-based MOFs (**2** and **4**) show significantly higher CO_2 uptakes and gated adsorption isotherms, dependent on activation conditions. Both these MOFs, loaded with MeOH, were activated at different temperatures, i.e., at 100, 150, and 200 °C. After each activation, the materials were monitored by IR spectroscopy, PXRD analysis, and gas adsorption measurements, i.e., at N_2 at 77 K and CO_2 at 195 K (Figures 3 and 4; Figures S22−S27).

The material **2MeOH** activated at 100 °C shows significant selectivity toward CO_2 versus N_2 with untypical isotherms, indicating the complex mechanism of stepwise CO_2 adsorption. Crystals of **2** maintain crystallinity and integrity during guest exchange, and the MeOH loaded structure of **2MeOH** was elucidated based on single-crystal X-ray diffraction (Figures S28−S31). It gave us deeper insight into subtle interactions within its crystal structure as well as allowed us to understand unusual adsorption properties. Assuming that the crystal structure of gently activated **2MeOH** (at 100 °C) corresponds to that of **2MeOH** (Figure S22), the observed three steps in the adsorption curves can be connected with sequential filling of pores (Table 1). In the first step ($p/p_0 \sim 0.09$; uptake = 92 $cm^3\ g^{-1}$) CO_2 freely diffuses into 1D channels and 0D cavities and fully fills them. Calculated total pore volume in **2MeOH** by Mercury software (after exclusion of solvent molecules) is equal to 0.167 $cm^3\ g^{-1}$, and it perfectly matches the experimental pore volume of 0.167 $cm^3\ g^{-1}$ (at $p/p_0 = 0.09$), calculated by Gurvich rule in this step. In the second step up to $p/p_0 \sim 0.43$ (uptake = 111 $cm^3\ g^{-1}$) CO_2 molecules infiltrate the framework and trigger structural changes which create additional interlayer voids. The experimental pore volume in this point is equal to 0.196 $cm^3\ g^{-1}$, which is nearly the same as the theoretical pore volume (0.194 $cm^3\ g^{-1}$) calculated for the structure of **2**. A further increase of pressure leads to the third distinguished step (at $p/p_0 = 0.59$; uptake = 130 $cm^3\ g^{-1}$) attributable to higher separation of layers and creation of additional space between them. The maximal pore volume of 0.244 $cm^3\ g^{-1}$ (at $p/p_0 \sim 1$) is 26% higher compared to the maximal theoretical pore volume calculated for **2** (0.194 $cm^3\ g^{-1}$).

Activation of **2MeOH** at higher temperatures (150 and 200 °C) leads to slight structural changes of the layered **2MeOH** which are associated with changes in the hydrogen bonding network. This is clearly manifested by PXRD patterns and IR spectra (both recorded at RT) of **2MeOH** conditioned at various temperatures for 1.5 h (Figure 3). The PXRD patterns mostly show signal broadening and slight shifts of major reflections, and the IR spectra provide evidence that these changes involve hydrogen bonding networks through the appearance or shift of bands corresponding to stretching C═O, N—H, and bending N—H vibrations. Whereas, the activation at 100 °C leaves the IR spectrum of **2MeOH** nearly intact; the spectra after activation at higher temperatures, in contrast, show significant shift of the $\nu(N{-}H)_{NH2iso}$ band from ca. 3382 to 3357 cm^{-1} as well as the appearance of new bands at 1655 and 1278 cm^{-1} corresponding to $\nu(C{=}O)$ and $\delta(N{-}H)$, respectively (Figure 3). The final confirmation is provided by CO_2 adsorption measurements that demonstrate one-step isotherms and much lower adsorption capacities (Figure 3) for the materials activated at higher temperatures.

The replacement of zinc in the synthesis of **2** by cadmium leads to formation of **4** that has different structure (Figures 1 and 2) and properties. The main differences between the two MOFs are as follows. First, the immersion of **4** in MeOH destroys the integrity of crystals and SC-XRD cannot be used to determinate the structure of **4MeOH**. Second, MOF **4** activated at 100 °C adsorbs both N_2 and CO_2 gases (Figure 4, Table 1). Third, the untypical CO_2 isotherm has a different shape, higher total uptake, and huge hysteresis loop (Figure 4). The isothermal adsorption−desorption cycle for N_2 at 77 K for **4MeOH** can be divided into three parts: (i) adsorption in the p/p_0 range of 0.00−0.37 which corresponds to diffusion-controlled filling of free voids by nitrogen, as corroborated by geometrical calculation based on crystal structure of **4** (Table 1, pore window size is comparable with kinetic diameter of N_2); (ii) adsorption at p/p_0 = 0.37−0.98 where additional space is created and derived experimental pore volume of 0.262 $cm^3\ g^{-1}$ surpasses the theoretical pore volume (0.184 $cm^3\ g^{-1}$) by ca. 42%; and (iii) desorption branch which indicates that N_2 molecules remain trapped in interlayer space up to low pressures.

Interesting adsorption properties of **4MeOH** are also observed for CO_2 at 195 K (Figure 4). The material activated at 100 °C adsorbs at 95 $cm^3\ g^{-1}$ in the low pressure region (at $p/p_0 = 1.2 \times 10^{-3}$). However, a further increase of pressure up to $p/p_0 = 0.43$ leads to only slightly increased uptake, reaching 108 $cm^3\ g^{-1}$. Therefore, in the entire region of p/p_0 = 0.0012−0.43 the CO_2 loaded structure remains stable and CO_2 occupies ca. 0.170−0.189 $cm^3\ g^{-1}$ pore volume, which corresponds to a theoretical pore volume of 0.184 $cm^3\ g^{-1}$, calculated for the crystal structure of **4**. The subsequent increase of pressure indicates structural transformation of **4MeOH** since two distinguished steps can be observed in the adsorption branch. These steps lead to the total uptake of 216 $cm^3\ g^{-1}$ at $p/p_0 \sim 1$ and the adsorbate must be accommodated in the increased interlayer space. In this point, the experimental pore volume is equal to 0.386 $cm^3\ g^{-1}$ which is higher by 110% compared to the theoretical pore volume obtained from the crystal structure (0.184 $cm^3\ g^{-1}$). Upon pressure release, a wide hysteresis in the desorption branch (within p/p_0 = 0.87−0.47) is observed which indicates strong interaction between CO_2 and the framework, most probably involving its NH/NH_2 groups. Moreover, similarly to the material **2MeOH**, the cadmium-based derivative **4MeOH** also shows activation-dependent adsorption characteristics. Increase of activation temperature to 150 °C or more disrupts initial interlayer hydrogen bonding network and the material loses flexible behavior toward CO_2 (Figure 4). It adsorbs considerably lower amounts of CO_2 (ca. 80 $cm^3\ g^{-1}$ for both applied activation temperatures) as well as N_2 (ca. 53 $cm^3\ g^{-1}$ for sample activated at 150 °C), whereby after activation at 200 °C it becomes nonporous toward N_2. The changes in hydrogen bonding in **4MeOH** upon activation at higher temperatures are evident from changes in the IR spectra of the activated materials which show significant shifts of $\nu(NH)$ bands by 18 cm^{-1} as compared to initial **4MeOH** (Figure 4). Further evidence of a subtle structural transformation upon activation at higher temperatures are provided by PXRD patterns which mostly show slight shifts of major reflections and confirm retention of crystallinity (Figure 4). The detailed comparison of the two aminoisophthalate-based structures suggests that pronounced differences in adsorption properties may originate from different layers arrangement, that is, ABC for **2** and ABCDEFG for **4** (Figure S6) and associated various hydrogen bond networks (Figure 2 and Figures S28−S30). Hydrogen bonding in **2MeOH** occurs between one NH_2 substituent of a $Zn_2(COO)_2$ unit and two *tdih* linkers from two adjacent layers.

https://dx.doi.org/10.1021/acs.inorgchem.0c01182
Inorg. Chem. 2020, 59, 10717−10726

One acylhydrazone group simultaneously works as a hydrogen bond donor and acceptor. In contrast, MOF **4** has a different hydrogen bonds arrangement, that is, not two but three *tdih* linkers interact with one amino substituent of a $Cd_2(COO)_2$ cluster.

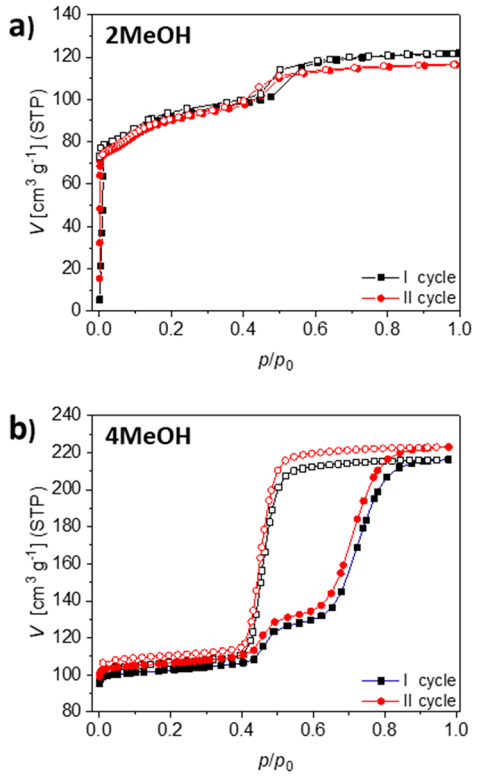

Figure 5. Stability of porosity upon repeated CO_2 adsorption (full symbols) and desorption (open symbols) at 195 K (a) for **2MeOH** and (b) for **4MeOH**. The materials were activated at 100 °C before the first adsorption−desorption cycle and at RT before the second cycle.

Numerous flexible MOFs are known to suffer from stress during activation and adsorption processes and resulting irreversible behavior. Thus, remarkable gated responses of **2MeOH** and **4MeOH** to CO_2 involving structural transformations prompted us to verify their reversibility. The second adsorption−desorption cycles were carried out, and both activated materials showed excellent reproducibility of the shapes of curves as well as the maximal uptakes different by no more than 5% from initial adsorption cycles (Figure 5).

CONCLUSION

We have synthesized and investigated the structure−adsorption property relationships of a series of four new layered flexible MOFs containing a diacylhydrazone linker. The interplay of metal centers and functionalization of isophthalate colinkers, together with dual capability of hydrogen bond formation of a diacylhydrazone, led to remarkable diversity of structures and properties in the series. In particular, pore dimensionalities of the acylhydrazone-based MOFs obtained were found to be mostly governed by different ionic radii of Zn^{2+} and Cd^{2+} ions. On the other hand, introducing of amino-substituted isophthalate colinkers and their interaction with the C═O groups of the acylhydrazone resulted in significant modification of interlayer hydrogen bonds which led to stepwise gated CO_2 adsorptions, not observed for unsubstituted isophthalate-based frameworks. The intriguing adsorption properties strongly depend on activation conditions of the materials, which were investigated by elemental and thermogravimetric analyses along with powder X-ray diffraction and IR spectroscopy. The work underscores the role of hydrogen bonds in crystal engineering of layered materials and the importance of activation conditions in such systems.

EXPERIMENTAL SECTION

Materials and Methods. Terephthalaldehyde di-isonicotinoylhydrazone (*tdih*) was prepared according to a published method.[56] All other reagents and solvents were of analytical grade (Sigma-Aldrich, POCH, Polmos) and were used without further purification.

Carbon, hydrogen, and nitrogen were determined by conventional microanalysis with the use of an Elementar Vario MICRO Cube elemental analyzer.

IR spectra were recorded on a Thermo Scientific Nicolet iS10 FT-IR spectrophotometer equipped with an iD7 diamond ATR attachment.

Thermogravimetric analyses (TGA) were performed on a Mettler-Toledo TGA/SDTA 851^e instrument at a heating rate of 10 °C min^{-1} in a temperature range of 25−600 °C (approximate sample weight of 20 mg). The measurements were performed at atmospheric pressure under argon flow. Also, for samples soaked in MeOH, TGA data were additionally measured on a Netzch STA 409 C/CD instrument at a heating rate of 10 °C min^{-1} in a temperature range of 25−600 °C (approximate sample weight of 50 mg; measurements were carried out under synthetic air).

Powder X-ray diffraction (PXRD) patterns were recorded at room temperature (295 K) on a Rigaku Miniflex 600 diffractometer with Cu−Kα radiation (λ = 1.5418 Å) in a 2θ range from 3° to 45° with a 0.02° step at a scan speed of 2.5° min^{-1}. Variable temperature powder X-ray diffraction (VT-PXRD) experiments were performed using Anton Paar BTS 500 heating stage from 30 to 350 °C. At each temperature samples were conditioned for 10 min prior to the measurement. Before *in situ* PXRD measurements, samples **2MeOH** and **4MeOH** were conditioned for 1.5 h at 100, 150, and 200 °C and cooled in a flow of inert gas (Ar). For samples prepared in this way, *ex-situ* ATR-IR spectra were measured.

PXRD patterns were additionally measured at room temperature on a STOE STADI P diffractometer using Cu−Kα1 radiation (λ = 1.5405 Å) and a 2D detector (Mythen, Dectris). Measurements on the STOE were performed in transmission geometry using a rotating flatbed sample holder.

Nitrogen and carbon dioxide adsorption/desorption studies were performed on a BELSORP-max adsorption apparatus (MicrotracBEL

Table 2. Elemental Analyses and Yields for Compounds 1−4

		$\{[Zn_2(iso)_2(tdih)_2]\cdot 4DMF\}_n$ **1**	$\{[Zn_2(NH_2iso)_2(tdih)_2]\cdot 2DMF\cdot 3H_2O\}_n$ **2**	$\{[Cd_2(iso)_2(tdih)_2]\cdot 5DMF\cdot H_2O\}_n$ **3**	$\{[Cd_2(NH_2iso)_2(tdih)_2]\cdot 4DMF\cdot H_2O\}_n$ **4**
formula		$C_{68}H_{68}N_{16}O_{16}Zn_2$	$C_{62}H_{62}N_{16}O_{17}Zn_2$	$C_{71}H_{77}N_{17}O_{18}Cd_2$	$C_{68}H_{72}N_{18}O_{17}Cd_2$
elem. anal. %	calcd	C 54.59; H 4.58; N 14.98	C 51.93; H 4.36; N 15.63	C 50.72; H 4.62; N 14.16	C 49.85; H 4.43; N 15.39
	found	C 54.68; H 4.26; N 14.72	C 51.86; H 4.20; N 15.63	C 50.90; H 4.12; N 13.64	C 49.79; H 3.81; N 15.25
yield (%)		64.0	74.9	70.8	74.4

https://dx.doi.org/10.1021/acs.inorgchem.0c01182
Inorg. Chem. 2020, 59, 10717−10726

Table 3. Elemental Analyses for $1H_2O$–$4H_2O$

		$\{[Zn_2(iso)_2(tdih)_2]\cdot 5H_2O\}_n$ **$1H_2O$**	$\{[Zn_2(NH_2iso)_2(tdih)_2]\cdot 13H_2O\}_n$ **$2H_2O$**	$\{[Cd_2(iso)_2(tdih)_2]\cdot 9H_2O\}_n$ **$3H_2O$**	$\{[Cd_2(NH_2iso)_2(tdih)_2]\cdot 8H_2O\}_n$ **$4H_2O$**
formula		$C_{56}H_{50}N_{12}O_{17}Zn_2$	$C_{56}H_{50}N_{14}O_{17}Zn_2$	$C_{56}H_{58}N_{12}O_{21}Cd_2$	$C_{56}H_{58}N_{14}O_{20}Cd_2$
elem. anal. %	calcd	C 52.98; H 3.83; N 14.08	C 45.82; H 4.67; N 13.36	C 46.07; H 4.00; N 11.51	C 45.69; H 3.97; N 13.66
	found	C 51.98; H 3.90; N 12.99	C 45.87; H 4.57; N 13.23	C 46.69; H 4.01; N 11.80	C 46.71; H, 3.82; N 13.66

Corp.). A temperature of 77 K was achieved by a liquid nitrogen bath and 195 K was achieved by dry ice/isopropanol bath. Prior to the sorption measurements, the samples **1**–**4** were soaked with MeOH for 1–2 days. After that, the samples were evacuated at different temperatures which are specified in the manuscript.

Syntheses. *Synthesis of $\{[M_2(Xiso)_2(tdih)_2]\cdot g\}_n$ materials (**1**–**4** and **3b**).* Terephthalaldehyde di-isonicotinoylhydrazone (*tdih*; 0.150 mmol), $M(NO_3)_2\cdot xH_2O$ (0.150 mmol) and a proper isophthalate acid (H_2Xiso) (0.150 mmol) were dissolved in DMF (14.4 mL) and H_2O (3.6 mL) by sonification (30 s) and heated in a sealed vial at 80 °C for 3 days. In the case of **3b**, 40% water (by volume) was used instead of 20%. Yellow (**1**, **3**, **3b**) or brown crystals (**2**, **4**) were filtered off, washed with DMF, and dried in oven at 60 °C for 0.5 h. Single crystals suitable for SC-XRD measurement were selected from the as-synthesized samples. Elemental analyses and synthetic yields for **1**–**4** are given in Table 2.

Stability Tests in Water. Each MOF **1**–**4** (50 mg) was soaked in 10 mL of water for 3 days at room temperature. After filtration, the samples (**$1H_2O$**–**$4H_2O$**) were washed with freshly distilled water and dried at 80 °C for 20 min. Each sample was analyzed by PXRD, IR, TGA and elemental analyses (see Table 3).

■ ASSOCIATED CONTENT

Supporting Information

The Supporting Information is available free of charge at https://pubs.acs.org/doi/10.1021/acs.inorgchem.0c01182.

IR spectra, PXRD patterns, TGA data, crystal structure drawings, additional sorption data, additional experimental data, and X-ray crystal data (PDF)

Accession Codes

CCDC 1877585, 1878988, 1898831, 1975135, 1975137, and 1993922 contain the supplementary crystallographic data for this paper. These data can be obtained free of charge via www.ccdc.cam.ac.uk/data_request/cif, or by emailing data_request@ccdc.cam.ac.uk, or by contacting The Cambridge Crystallographic Data Centre, 12 Union Road, Cambridge CB2 1EZ, UK; fax: +44 1223 336033.

■ AUTHOR INFORMATION

Corresponding Author

Dariusz Matoga – *Faculty of Chemistry, Jagiellonian University, 30-387 Kraków, Poland;* orcid.org/0000-0002-0064-5541; Email: dariusz.matoga@uj.edu.pl

Authors

Kornel Roztocki – *Faculty of Chemistry, Jagiellonian University, 30-387 Kraków, Poland*

Monika Szufla – *Faculty of Chemistry, Jagiellonian University, 30-387 Kraków, Poland*

Volodymyr Bon – *Department of Inorganic Chemistry, Technische Universität Dresden, 01062 Dresden, Germany;* orcid.org/0000-0002-9851-5031

Irena Senkovska – *Department of Inorganic Chemistry, Technische Universität Dresden, 01062 Dresden, Germany;* orcid.org/0000-0001-7052-1029

Stefan Kaskel – *Department of Inorganic Chemistry, Technische Universität Dresden, 01062 Dresden, Germany;* orcid.org/0000-0003-4572-0303

Complete contact information is available at: https://pubs.acs.org/10.1021/acs.inorgchem.0c01182

Notes

The authors declare no competing financial interest.

■ ACKNOWLEDGMENTS

The National Science Centre (NCN, Poland) is gratefully acknowledged for the financial support (2015/17/B/ST5/01190) of this research. K.R. additionally thanks the National Science Centre (NCN, Poland) for a doctoral scholarship within the ETIUDA funding scheme (2018/28/T/ST5/00333). Dr. M. Hodorowicz is acknowledged for non-synchrotron-based SC-XRD measurements. The research was carried out partially with the equipment purchased thanks to the financial support of the European Regional Development Fund in the framework of the Polish Innovation Economy Operational Program (contract no. POIG.02.01.00-12-023/08).

■ REFERENCES

(1) Zhang, L.; Bailey, J. B.; Subramanian, R. H.; Groisman, A.; Tezcan, F. A. Hyperexpandable, Self-Healing Macromolecular Crystals with Integrated Polymer Networks. *Nature* **2018**, *557*, 86–91.

(2) Biradha, K.; Fujita, M. A Springlike 3D-Coordination Network That Shrinks or Swells in a Crystal-to-Crystal Manner upon Guest Removal or Readsorption. *Angew. Chem., Int. Ed.* **2002**, *41*, 3392–3395.

(3) Huang, H.-L.; Lin, H.-Y.; Chen, P.-S.; Lee, J.-J.; Kung, H.-C.; Wang, S.-L. A Highly Flexible Inorganic Framework with Amphiphilic Amine Assemblies as Templates. *Dalton Trans.* **2017**, *46*, 364–368.

(4) Reddy, C. M.; Padmanabhan, K. A.; Desiraju, G. R. Structure-Property Correlations in Bending and Brittle Organic Crystals. *Cryst. Growth Des.* **2006**, *6*, 2720–2731.

(5) Takamizawa, S.; Takasaki, Y. Superelastic Shape Recovery of Mechanically Twinned 3,5-Difluorobenzoic Acid Crystals. *Angew. Chem., Int. Ed.* **2015**, *54*, 4815–4817.

(6) Owczarek, M.; Hujsak, K. A.; Ferris, D. P.; Prokofjevs, A.; Majerz, I.; Szklarz, P.; Zhang, H.; Sarjeant, A. A.; Stern, C. L.; Jakubas, R.; Hong, S.; Dravid, V. P.; Stoddart, J. F. Flexible Ferroelectric Organic Crystals. *Nat. Commun.* **2016**, *7*, 13108.

(7) Kitagawa, D.; Kobatake, S. Crystal Thickness Dependence of Photoinduced Crystal Bending of 1,2-Bis(2-Methyl-5-(4-(1-Naphthoyloxymethyl)Phenyl)-3-Thienyl)Perfluorocyclopentene. *J. Phys. Chem. C* **2013**, *117*, 20887–20892.

(8) Kitagawa, S.; Kitaura, R.; Noro, S. Functional Porous Coordination Polymers. *Angew. Chem., Int. Ed.* **2004**, *43*, 2334–2375.

(9) Schneemann, A.; Bon, V.; Schwedler, I.; Senkovska, I.; Kaskel, S.; Fischer, R. A. Flexible Metal-Organic Frameworks. *Chem. Soc. Rev.* **2014**, *43*, 6062–6096.

(10) Chang, Z.; Yang, D.-H.; Xu, J.; Hu, T.-L.; Bu, X.-H. Flexible Metal-Organic Frameworks: Recent Advances and Potential Applications. *Adv. Mater.* **2015**, *27*, 5432–5441.

(11) Halder, A.; Ghoshal, D. Structure and Properties of Dynamic Metal-Organic Frameworks: A Brief Accounts of Crystalline-to-Crystalline and Crystalline-to-Amorphous Transformations. *CrystEngComm* **2018**, *20*, 1322−1345.
(12) Mellot-Draznieks, C.; Serre, C.; Surblé, S.; Audebrand, N.; Férey, G. Very Large Swelling in Hybrid Frameworks: A Combined Computational and Powder Diffraction Study. *J. Am. Chem. Soc.* **2005**, *127*, 16273−16278.
(13) Loiseau, T.; Serre, C.; Huguenard, C.; Fink, G.; Taulelle, F.; Henry, M.; Bataille, T.; Férey, G. A Rationale for the Large Breathing of the Porous Aluminum Terephthalate (MIL-53) Upon Hydration. *Chem. - Eur. J.* **2004**, *10*, 1373−1382.
(14) Fairen-Jimenez, D.; Moggach, S. A.; Wharmby, M. T.; Wright, P. A.; Parsons, S.; Düren, T. Opening the Gate: Framework Flexibility in ZIF-8 Explored by Experiments and Simulations. *J. Am. Chem. Soc.* **2011**, *133*, 8900−8902.
(15) Krause, S.; Bon, V.; Senkovska, I.; Stoeck, U.; Wallacher, D.; Többens, D. M.; Zander, S.; Pillai, R. S.; Maurin, G.; Coudert, F.-X.; Kaskel, S. A Pressure-Amplifying Framework Material with Negative Gas Adsorption Transitions. *Nature* **2016**, *532*, 348.
(16) Shivanna, M.; Yang, Q.-Y.; Bajpai, A.; Patyk-Kazmierczak, E.; Zaworotko, M. J. A Dynamic and Multi-Responsive Porous Flexible Metal-Organic Material. *Nat. Commun.* **2018**, *9*, 3080.
(17) Maji, T. K.; Matsuda, R.; Kitagawa, S. A Flexible Interpenetrating Coordination Framework with a Bimodal Porous Functionality. *Nat. Mater.* **2007**, *6*, 142−148.
(18) Kondo, A.; Noguchi, H.; Ohnishi, S.; Kajiro, H.; Tohdoh, A.; Hattori, Y.; Xu, W.-C.; Tanaka, H.; Kanoh, H.; Kaneko, K. Novel Expansion/Shrinkage Modulation of 2D Layered MOF Triggered by Clathrate Formation with CO2Molecules. *Nano Lett.* **2006**, *6*, 2581−2584.
(19) Horike, S.; Tanaka, D.; Nakagawa, K.; Kitagawa, S. Selective Guest Sorption in an Interdigitated Porous Framework with Hydrophobic Pore Surfaces. *Chem. Commun.* **2007**, No. 32, 3395−3397.
(20) Roztocki, K.; Jędrzejowski, D.; Hodorowicz, M.; Senkovska, I.; Kaskel, S.; Matoga, D. Isophthalate-Hydrazone 2D Zinc-Organic Framework: Crystal Structure, Selective Adsorption, and Tuning of Mechanochemical Synthetic Conditions. *Inorg. Chem.* **2016**, *55*, 9663−9670.
(21) Cheng, Y.; Kajiro, H.; Noguchi, H.; Kondo, A.; Ohba, T.; Hattori, Y.; Kaneko, K.; Kanoh, H. Tuning of Gate Opening of an Elastic Layered Structure MOF in CO2 Sorption with a Trace of Alcohol Molecules. *Langmuir* **2011**, *27*, 6905−6909.
(22) Mason, J. A.; Oktawiec, J.; Taylor, M. K.; Hudson, M. R.; Rodriguez, J.; Bachman, J. E.; Gonzalez, M. I.; Cervellino, A.; Guagliardi, A.; Brown, C. M.; Llewellyn, P. L.; Masciocchi, N.; Long, J. R. Methane Storage in Flexible Metal-Organic Frameworks with Intrinsic Thermal Management. *Nature* **2015**, *527*, 357.
(23) Katsoulidis, A. P.; Antypov, D.; Whitehead, G. F. S.; Carrington, E. J.; Adams, D. J.; Berry, N. G.; Darling, G. R.; Dyer, M. S.; Rosseinsky, M. J. Chemical Control of Structure and Guest Uptake by a Conformationally Mobile Porous Material. *Nature* **2019**, *565*, 213−217.
(24) Carrington, E. J.; McAnally, C. A.; Fletcher, A. J.; Thompson, S. P.; Warren, M.; Brammer, L. Solvent-Switchable Continuous-Breathing Behaviour in a Diamondoid Metal-Organic Framework and Its Influence on CO2 versus CH4 Selectivity. *Nat. Chem.* **2017**, *9*, 882.
(25) Roztocki, K.; Formalik, F.; Krawczuk, A.; Senkovska, I.; Kuchta, B.; Kaskel, S.; Matoga, D. Collective Breathing in an Eightfold Interpenetrated Metal-Organic Framework: From Mechanistic Understanding towards Threshold Sensing Architectures. *Angew. Chem., Int. Ed.* **2020**, *59*, 4491−4497.
(26) Sato, H.; Kosaka, W.; Matsuda, R.; Hori, A.; Hijikata, Y.; Belosludov, R. V.; Sakaki, S.; Takata, M.; Kitagawa, S. Self-Accelerating CO Sorption in a Soft Nanoporous Crystal. *Science* **2014**, *343*, 167−170.
(27) Sakata, Y.; Furukawa, S.; Kondo, M.; Hirai, K.; Horike, N.; Takashima, Y.; Uehara, H.; Louvain, N.; Meilikhov, M.; Tsuruoka, T.; Isoda, S.; Kosaka, W.; Sakata, O.; Kitagawa, S. Shape-Memory Nanopores Induced in Coordination Frameworks by Crystal Downsizing. *Science* **2013**, *339*, 193−196.
(28) Yang, F.; Xu, G.; Dou, Y.; Wang, B.; Zhang, H.; Wu, H.; Zhou, W.; Li, J.-R.; Chen, B. A Flexible Metal-Organic Framework with a High Density of Sulfonic Acid Sites for Proton Conduction. *Nat. Energy* **2017**, *2*, 877−883.
(29) Maspoch, D.; Ruiz-Molina, D.; Wurst, K.; Domingo, N.; Cavallini, M.; Biscarini, F.; Tejada, J.; Rovira, C.; Veciana, J. A Nanoporous Molecular Magnet with Reversible Solvent-Induced Mechanical and Magnetic Properties. *Nat. Mater.* **2003**, *2*, 190−195.
(30) Shearer, G. C.; Chavan, S.; Ethiraj, J.; Vitillo, J. G.; Svelle, S.; Olsbye, U.; Lamberti, C.; Bordiga, S.; Lillerud, K. P. Tuned to Perfection: Ironing Out the Defects in Metal-Organic Framework UiO-66. *Chem. Mater.* **2014**, *26*, 4068−4071.
(31) Øien, S.; Agostini, G.; Svelle, S.; Borfecchia, E.; Lomachenko, K. A.; Mino, L.; Gallo, E.; Bordiga, S.; Olsbye, U.; Lillerud, K. P.; Lamberti, C. Probing Reactive Platinum Sites in UiO-67 Zirconium Metal-Organic Frameworks. *Chem. Mater.* **2015**, *27*, 1042−1056.
(32) Vitillo, J. G.; Lescouet, T.; Savonnet, M.; Farrusseng, D.; Bordiga, S. Soft Synthesis of Isocyanate-Functionalised Metal-Organic Frameworks. *Dalton Trans.* **2012**, *41*, 14236−14238.
(33) Bloch, E. D.; Hudson, M. R.; Mason, J. A.; Chavan, S.; Crocellà, V.; Howe, J. D.; Lee, K.; Dzubak, A. L.; Queen, W. L.; Zadrozny, J. M.; Geier, S. J.; Lin, L.-C.; Gagliardi, L.; Smit, B.; Neaton, J. B.; Bordiga, S.; Brown, C. M.; Long, J. R. Reversible CO Binding Enables Tunable CO/H2 and CO/N2 Separations in Metal-Organic Frameworks with Exposed Divalent Metal Cations. *J. Am. Chem. Soc.* **2014**, *136*, 10752−10761.
(34) Matoga, D.; Gil, B.; Nitek, W.; Todd, A. D.; Bielawski, C. W. Dynamic 2D Manganese(II) Isonicotinate Framework with Reversible Crystal-to-Amorphous Transformation and Selective Guest Adsorption. *CrystEngComm* **2014**, *16*, 4959−4962.
(35) McDonald, T. M.; Mason, J. A.; Kong, X.; Bloch, E. D.; Gygi, D.; Dani, A.; Crocellà, V.; Giordanino, F.; Odoh, S. O.; Drisdell, W. S.; Vlaisavljevich, B.; Dzubak, A. L.; Poloni, R.; Schnell, S. K.; Planas, N.; Lee, K.; Pascal, T.; Wan, L. F.; Prendergast, D.; Neaton, J. B.; Smit, B.; Kortright, J. B.; Gagliardi, L.; Bordiga, S.; Reimer, J. A.; Long, J. R. Cooperative Insertion of CO2 in Diamine-Appended Metal-Organic Frameworks. *Nature* **2015**, *519*, 303−308.
(36) Matoga, D.; Oszajca, M.; Molenda, M. Ground to Conduct: Mechanochemical Synthesis of a Metal-Organic Framework with High Proton Conductivity. *Chem. Commun.* **2015**, *51*, 7637−7640.
(37) Matoga, D.; Roztocki, K.; Wilke, M.; Emmerling, F.; Oszajca, M.; Fitta, M.; Balanda, M. Crystalline Bilayers Unzipped and Rezipped: Solid-State Reaction Cycle of a Metal-Organic Framework with Triple Rearrangement of Intralayer Bonds. *CrystEngComm* **2017**, *19*, 2987−2995.
(38) Nishida, J.; Tamimi, A.; Fei, H.; Pullen, S.; Ott, S.; Cohen, S. M.; Fayer, M. D. Structural Dynamics inside a Functionalized Metal-Organic Framework Probed by Ultrafast 2D IR Spectroscopy. *Proc. Natl. Acad. Sci. U. S. A.* **2014**, *111*, 18442−18447.
(39) Schneider, C.; Ukaj, D.; Koerver, R.; Talin, A. A.; Kieslich, G.; Pujari, S. P.; Zuilhof, H.; Janek, J.; Allendorf, M. D.; Fischer, R. A. High Electrical Conductivity and High Porosity in a Guest@MOF Material: Evidence of TCNQ Ordering within Cu3BTC2Micropores. *Chem. Sci.* **2018**, *9*, 7405−7412.
(40) Borfecchia, E.; Maurelli, S.; Gianolio, D.; Groppo, E.; Chiesa, M.; Bonino, F.; Lamberti, C. Insights into Adsorption of NH3 on HKUST-1 Metal-Organic Framework: A Multitechnique Approach. *J. Phys. Chem. C* **2012**, *116*, 19839−19850.
(41) Hoffman, A. E. J.; Vanduyfhuys, L.; Nevjestić, I.; Wieme, J.; Rogge, S. M. J.; Depauw, H.; Van Der Voort, P.; Vrielinck, H.; Van Speybroeck, V. Elucidating the Vibrational Fingerprint of the Flexible Metal-Organic Framework MIL-53(Al) Using a Combined Experimental/Computational Approach. *J. Phys. Chem. C* **2018**, *122*, 2734−2746.

https://dx.doi.org/10.1021/acs.inorgchem.0c01182
Inorg. Chem. 2020, 59, 10717−10726

(42) Roztocki, K.; Jędrzejowski, D.; Hodorowicz, M.; Senkovska, I.; Kaskel, S.; Matoga, D. Effect of Linker Substituent on Layers Arrangement, Stability, and Sorption of Zn-Isophthalate/Acylhydrazone Frameworks. *Cryst. Growth Des.* **2018**, *18*, 488−497.
(43) Roztocki, K.; Lupa, M.; Sławek, A.; Makowski, W.; Senkovska, I.; Kaskel, S.; Matoga, D. Water-Stable Metal-Organic Framework with Three Hydrogen-Bond Acceptors: Versatile Theoretical and Experimental Insights into Adsorption Ability and Thermo-Hydrolytic Stability. *Inorg. Chem.* **2018**, *57*, 3287−3296.
(44) Ehrling, S.; Senkovska, I.; Bon, V.; Evans, J. D.; Petkov, P.; Krupskaya, Y.; Kataev, V.; Wulf, T.; Krylov, A.; Vtyurin, A.; Krylova, S.; Adichtchev, S.; Slyusareva, E.; Weiss, M. S.; Büchner, B.; Heine, T.; Kaskel, S. Crystal Size versus Paddle Wheel Deformability: Selective Gated Adsorption Transitions of the Switchable Metal-Organic Frameworks DUT-8(Co) and DUT-8(Ni). *J. Mater. Chem. A* **2019**, *7*, 21459−21475.
(45) Park, H. J.; Suh, M. P. Stepwise and Hysteretic Sorption of N2, O2, CO2, and H2 Gases in a Porous Metal-Organic Framework [Zn2(BPnDC)2(Bpy)]. *Chem. Commun.* **2010**, *46*, 610−612.
(46) Bon, V.; Senkovska, I.; Wallacher, D.; Többens, D. M.; Zizak, I.; Feyerherm, R.; Mueller, U.; Kaskel, S. In Situ Observation of Gating Phenomena in the Flexible Porous Coordination Polymer Zn2(BPnDC)2(Bpy) (SNU-9) in a Combined Diffraction and Gas Adsorption Experiment. *Inorg. Chem.* **2014**, *53*, 1513−1520.
(47) Tian, L.; Chen, Z.; Yu, A.; Song, H.-B.; Cheng, P. Novel Flexible Bis-Triazole Bridged Copper(Ii) Coordination Polymers Varying from One- to Three-Dimensionality. *CrystEngComm* **2012**, *14*, 2032−2039.
(48) Rebilly, J.-N.; Bacsa, J.; Rosseinsky, M. J. 1D Tubular and 2D Metal-Organic Frameworks Based on a Flexible Amino Acid Derived Organic Spacer. *Chem. - Asian J.* **2009**, *4*, 892−903.
(49) Cheng, J.; Chen, S.; Chen, D.; Dong, L.; Wang, J.; Zhang, T.; Jiao, T.; Liu, B.; Wang, H.; Kai, J.-J.; Zhang, D.; Zheng, G.; Zhi, L.; Kang, F.; Zhang, W. Editable Asymmetric All-Solid-State Supercapacitors Based on High-Strength, Flexible, and Programmable 2D-Metal-Organic Framework/Reduced Graphene Oxide Self-Assembled Papers. *J. Mater. Chem. A* **2018**, *6*, 20254−20266.
(50) Bloch, W. M.; Doonan, C. J.; Sumby, C. J. Tuning Packing, Structural Flexibility, and Porosity in 2D Metal-Organic Frameworks by Metal Node Choice. *Aust. J. Chem.* **2019**, *72*, 797−804.
(51) Leszczyński, M. K.; Justyniak, I.; Gontarczyk, K.; Lewiński, J. Solvent Templating and Structural Dynamics of Fluorinated 2D Cu-Carboxylate MOFs Derived from the Diffusion-Controlled Process. *Inorg. Chem.* **2020**, *59*, 4389−4396.
(52) Kongshaug, K. O.; Fjellvåg, H. Design of Novel Bilayer Compounds of the CPO-8 Type Containing 1D Channels. *Inorg. Chem.* **2006**, *45*, 2424−2429.
(53) Blatov, V. A.; Shevchenko, A. P.; Proserpio, D. M. Applied Topological Analysis of Crystal Structures with the Program Package ToposPro. *Cryst. Growth Des.* **2014**, *14*, 3576−3586.
(54) Greathouse, J. A.; Allendorf, M. D. The Interaction of Water with MOF-5 Simulated by Molecular Dynamics. *J. Am. Chem. Soc.* **2006**, *128*, 10678−10679.
(55) Willems, T. F.; Rycroft, C. H.; Kazi, M.; Meza, J. C.; Haranczyk, M. Algorithms and Tools for High-Throughput Geometry-Based Analysis of Crystalline Porous Materials. *Microporous Mesoporous Mater.* **2012**, *149*, 134−141.
(56) Roztocki, K.; Szufla, M.; Hodorowicz, M.; Senkovska, I.; Kaskel, S.; Matoga, D. Introducing a Longer versus Shorter Acylhydrazone Linker to a Metal-Organic Framework: Parallel Mechanochemical Approach, Nonisoreticular Structures, and Diverse Properties. *Cryst. Growth Des.* **2019**, *19*, 7160−7169.

https://dx.doi.org/10.1021/acs.inorgchem.0c01182
Inorg. Chem. 2020, 59, 10717−10726